The Astrophysical Journal, 654:938–944, 2007 January 10

A NEAR-INFRARED AND X-RAY STUDY OF W49 B: A WIND CAVITY EXPLOSION

Jonathan W. Keohane,[1,2] William T. Reach,[2] Jeonghee Rho,[2] and Thomas H. Jarrett[2]
Received 2004 July 20; accepted 2006 September 1

ABSTRACT

We present near-infrared narrowband images of the supernova remnant W49 B, taken with the WIRC instrument on the Hale 200 inch (5 m) telescope on Mount Palomar. The 1.64 μm [Fe II] image reveals a barrel-shaped structure with coaxial rings, which is suggestive of bipolar wind structures surrounding massive stars. The 2.12 μm shocked molecular hydrogen image extends 1.9 pc outside of the [Fe II] emission to the southeast. We also present archival *Chandra* data, which show an X-ray jetlike structure along the axis of the [Fe II] barrel, flaring at each end. Fitting single-temperature X-ray emission models reveals an enhancement of heavy elements, with particularly high abundances of hot Fe and Ni, and relatively metal-rich core and jet regions. We interpret these findings as evidence that W49 B originated inside a wind-blown bubble ($R \sim 5$ pc) inside a dense molecular cloud. This suggests that W49 B's progenitor was a supermassive star that could significantly shape its surrounding environment. We also suggest two interpretations for the jet morphology, abundance variations, and molecular hydrogen emission: (1) the explosion may have been jet driven, interacting with the molecular cavity (i.e., a gamma-ray burst); or (2) the explosion could have been a traditional supernova, with the jet structure being the result of interactions between the shock and an enriched interstellar cloud.

Subject headings: circumstellar matter — gamma rays: bursts — infrared: ISM — supernova remnants — supernovae: individual (W49 B) — X-rays: ISM

1. INTRODUCTION

W49 B (G43.3-0.2) has the highest radio surface brightness of all mixed-morphology supernova remnants (SNRs) in the Galaxy (Pye et al. 1984; Moffett & Reynolds 1994). SNRs exhibiting centrally filled X-rays inside an edge-brightened radio shell are referred to as mixed-morphology (Rho & Petre 1998). A number of models have been proposed for mixed-morphology supernova remnants (White & Long 1991; Cox et al. 1999; Shelton et al. 1999; Chevalier 1999); these models were designed to explain the larger (i.e., older) SNRs by invoking interactions with a denser than average interstellar medium. The very high radio brightness and the X-ray properties of W49 B make it a compelling object to study in detail, because it may be fundamentally different from other remnants of its class.

High-resolution X-ray spectra of W49 B (Hwang et al. 2000) revealed elemental abundances enhanced in heavy elements, suggesting that W49 B was the product of a Type Ia explosion. However, a subsequent study of H I absorption (Brogan & Troland 2001) shows that W49 B is at the same distance as the star-forming region W49 A (11.4 kpc; Gwinn et al. 1992). Moreover, long-wavelength radio observations (Lacey et al. 2001) suggest that W49 B is absorbed by H^+ gas and is in a high-pressure ($\sim 10^6$ cm^{-3} K) region of the Galaxy, again associating the remnant with the W49 A complex. But at this distance, W49 B would have to have a massive progenitor, more akin to a Type II supernova. Thus, we have an observational inconsistency: W49 B has enhanced iron abundances, which are characteristic of a Type Ia supernova, yet it is located in a star-forming region and is more likely the result of a core-collapse explosion.

Recently, Miceli et al. (2006) completed a study of W49 B with *XMM-Newton* in which they concluded that the X-ray emission arises in a high-metallicity collisionally ionized plasma, with a temperature gradient from west to east.

In this paper we present near-infrared narrow-line imaging (§ 2.1), which we compare to our spectral analysis of *Chandra* archival data (§ 2.2). In § 3 we interpret our results as evidence that W49 B was created inside a wind-blown bubble within a molecular cloud. We also include two very different interpretations of our observations: (1) in § 3.1 we interpret our observations as consistent with a jet-driven explosion (i.e., a gamma-ray burst), and in § 3.2 we interpret our observations as the result of a traditional supernova explosion inside a complex cavity.

2. ANALYSIS

2.1. *Near-Infrared Observations*

We observed W49 B on 2003 August 9 and 10 with the Hale 5 m telescope on Mount Palomar under clear skies, using the new Wide Field Infrared Camera (the WIRC; Wilson et al. 2003). The WIRC is a 2048 × 2048 Rockwell Hawaii-II near-infrared (NIR) detector mounted at the f/3.3 prime focus, resulting in an 8.7′ field of view with 0.25″ pixels.

We observed W49 B with four filters (see Table 1): two narrow-line filters and two continuum filters in the 1.6–2.2 μm window. The purpose of the K_s continuum observation was to search for synchrotron emission from W49 B, which was not observed. With each filter, we alternated observing on and off our source, with each on-source observation located at a slightly different position, providing a good sampling our object as well as the nearby off-source sky.

Because the WIRC is a new instrument, we developed our own IRAF package to implement the following procedure independently for each filter: (1) we subtracted off the median dark image with corresponding frame times from each image and corrected for the nonlinear response of the detector; (2) we pixel-by-pixel median averaged our off-source images, with the highest two values rejected to eliminate stars to form a "sky image"; (3) we

[1] Department of Physics and Astronomy, Hampden-Sydney College, Hampden Sydney, VA.
[2] *Spitzer* Science Center, California Institute of Technology, Pasadena, CA.

TABLE 1
WIRC Observing Log for W49 B

Filter	Exposure (s)	Pointings	Seeing (arcsec)	Air Mass	Total Time (minutes)
H_2	3×30	7	0.7	1.34	10.5
K_{cont}	3×30	1	0.7	1.49	1.5
Fe II	2×45	7	0.8	1.16	10.5
K_s	6×10	12	0.7	1.38	12.0

subtracted the sky image off each of our source images; (4) we divided this image by a standard flat derived from the linear response of each pixel; (5) we subtracted a single median off-source background level; (6) we corrected for cross-field flux bias; (7) we applied a world coordinate system to our images using the Two Micron All Sky Survey (2MASS) point-source catalog; (8) we flux calibrated our images using the 2MASS point-source catalog; (9) we mosaicked our images; (10) we resubtracted the ambient background level; and (11) we applied a final calibration using the 2MASS point-source catalog. The photometric uncertainty was ~7% for the spectral line observations and ~6% for K_s, and primarily limited by stellar confusion noise.

The total narrowband infrared flux densities are 30 Jy (mag = 3.4, $L = 1 \times 10^{37}$ ergs s^{-1}) in H_2 and 61 Jy (mag = 3.1, $L = 3 \times 10^{37}$ ergs s^{-1}) in [Fe II]. We used these values to estimate the mass of Fe^+ ions and H_2 molecules using multilevel excitation models and a wide range of physically reasonable excitation conditions, including all path lengths shorter than the remnant diameter, all reasonable temperatures for the observed ionization state, and pressures less than 1000 times the typical interstellar value (see also Rho et al. 2001). Thus, the mass of Fe^+ must be between 0.2 and 20 $M_\odot$, with the lower and higher masses corresponding to electron (temperature, density) of (1000 K, 8000 cm^{-3}) and (700 K, 1600 cm^{-3}), respectively. For H_2, the mass is between 14 and 550 $M_\odot$, with the lower and higher masses corresponding to H_2 (temperature, density) of (2000 K, 2000 cm^{-3}) and (1200 K, 3000 cm^{-3}), respectively.

Our calibrated H_2 and [Fe II] images are shown as red and green, respectively, in Figure 1, while the *Chandra* image is blue. This figure shows molecular hydrogen emission well outside the other emission, especially in the southeast. The [Fe II] emission appears to be coaxial rings, defining an elongated shell. The *Chandra* X-ray emission (see § 2.2 below) is inside the NIR emission, stopping at approximately the same location as the [Fe II]. We interpret these data as evidence that W49 B was a cavity explosion, as discussed below in § 3.

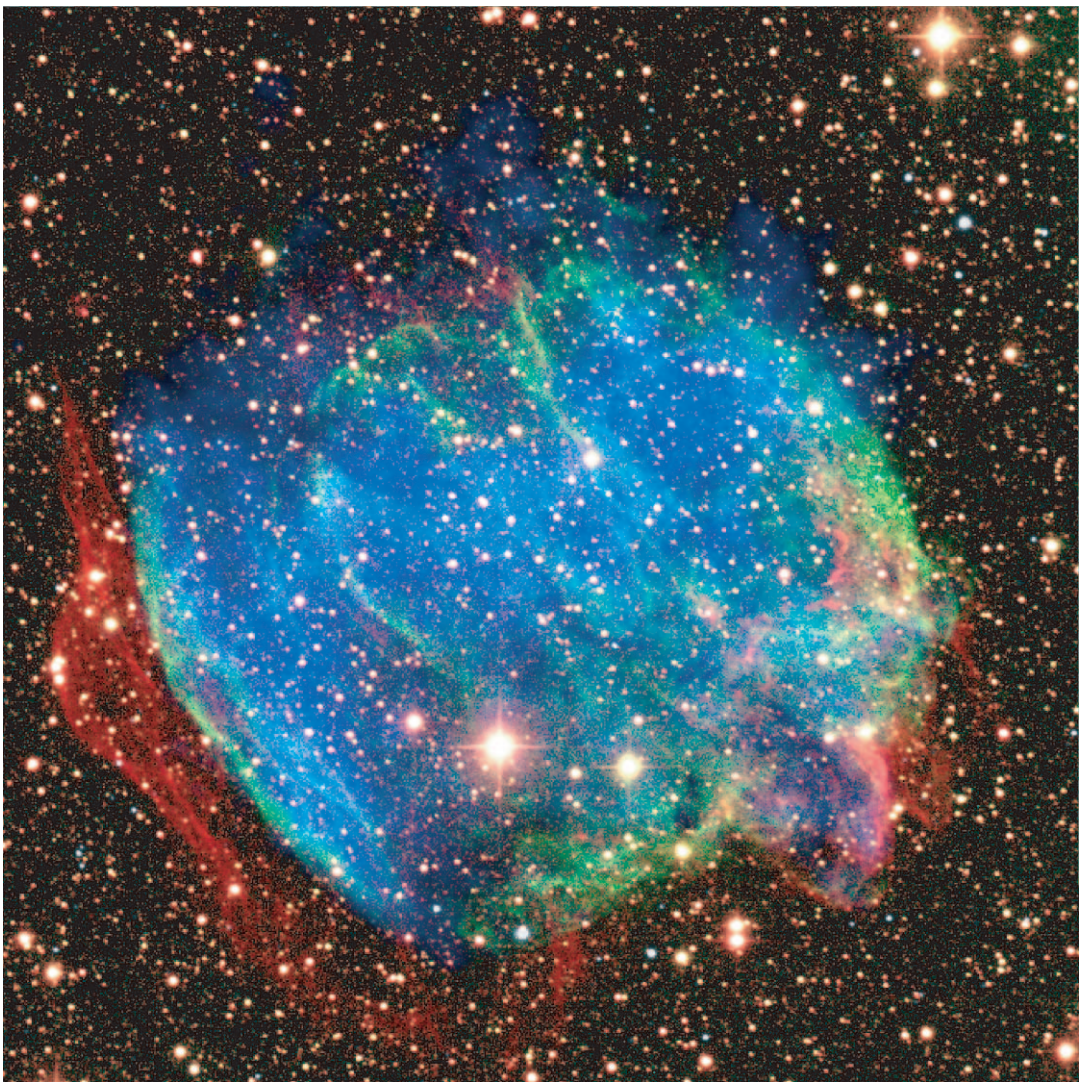

Fig. 1.—H_2 (*red*), [Fe II] (*green*), and X-ray (*blue*) color composite image of W49 B. The K_s image was also included as white, in order to produce white foreground stars.

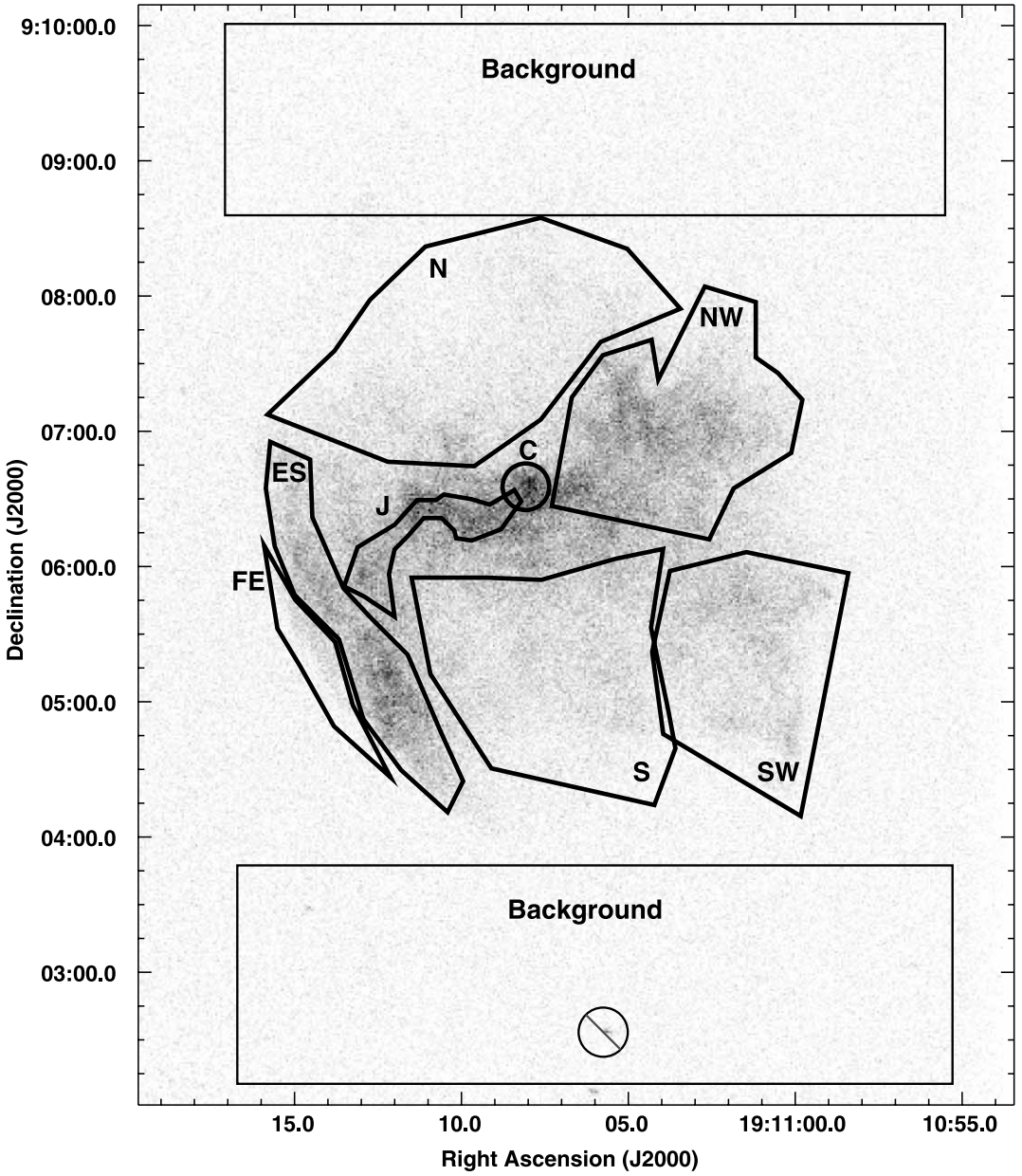

FIG. 2.—*Chandra* image of W49 B, with spectral extraction regions overlaid. The regions are named from east to west: FE (far east), ES (east shell), J (jet), C (center), N (north), S (south), NW (northwest), and SW (southwest). The approximate central R.A. and declination are also shown in Table 2.

2.2. *Chandra Archival Data*

The *Chandra* X-ray Observatory performed a 55 ks observation of W49 B in 2000 July (PI: S. S. Holt; Petre et al. 2000; Stahle et al. 2001), and the data became public a year later. Morphologically, these data show a double T-shaped structure aligned with the rotation axis of the progenitor star, as discussed above in § 2.1 (see Fig. 1).

We obtained screened events files from the *Chandra* Supernova Remnant Catalog (Seward et al. 2004).[3] Using standard analysis techniques,[4] we extracted spectra from the regions shown in Figure 2 and made weighted response functions using the ACISSPEC script. The data are best fit using an absorbed (WABS; Morrison & McCammon 1983) single-temperature model (VMEKAL; Mewe et al. 1985, 1986; Liedahl et al. 1995). The VMEKAL model does not appear to be a perfect fit; it underpredicts the 1.865 keV line emission from He-like Si (Si^{12+}) and does include some spectral features between the Ca and Fe lines (also seen by Hwang et al. 2000). Nevertheless, it is a reasonably good fit overall. We also fit a non-ionization equilibrium model (i.e., VNEI; Hamilton et al. 1983), which fared no better than the VMEKAL model ($nt > 10^4$ cm^{-3} yr), implying that the gas is close to collisional ionization equilibrium.

Like Hwang et al. (2000), we observe an overall overabundance of heaver elements. Moreover, note from Table 2 the overall trend toward higher metallic abundances in the center, jet, and eastern shell, as opposed to the outer regions of W49 B. This same

[3] Catalog available at http://srao.snu.ac.kr/SNRCAT/CHANDRASNR/.
[4] See http://cxc.harvard.edu/ciao/.

TABLE 2
X-Ray Spectral Fit Parameters by Region

Parameter	Center	Jet	East Shell	Far East	North	Southwest	South	Northwest	All[a]
R.A.	19 11 08	19 11 11	19 11 13	19 11 14	19 11 09	19 11 01	19 11 07	19 11 03	...
Decl.	9 06 40	9 60 30	9 05 45	9 05 30	9 07 45	9 05 30	9 05 15	9 07 00	...
N_H[b]	5.5 ± 0.4	5.5 ± 0.2	5.1 ± 0.2	4.8 ± 0.5	5.0 ± 0.2	5.8 ± 0.2	5.3 ± 0.2	5.2 ± 0.1	5.18 ± 0.05
kT[c]	1.6 ± 0.1	1.74 ± 0.06	1.66 ± 0.04	1.4 ± 0.2	1.57 ± 0.05	1.33 ± 0.05	1.32 ± 0.04	1.53 ± 0.04	1.58 ± 0.02
$\int n_e n_H dV$[d]	140^{+60}_{-90}	510 ± 100	1300 ± 200	160 ± 70	1200 ± 200	2800 ± 300	3500 ± 300	4400 ± 300	16100 ± 500
Si[e]	7^{+8}_{-3}	$4.5^{+1.4}_{-0.9}$	2.8 ± 0.4	2^{+2}_{-1}	2.0 ± 0.4	1.1 ± 0.2	1.1 ± 0.2	1.4 ± 0.2	1.84 ± 0.08
S [e]	4^{+8}_{-2}	$3.6^{+1.0}_{-0.7}$	2.8 ± 0.4	2^{+2}_{-1}	2.0 ± 0.3	1.2 ± 0.2	1.0 ± 0.2	1.35 ± 0.10	1.83 ± 0.07
Ar[e]	4^{+8}_{-2}	4 ± 1	2.5 ± 0.4	$1.1^{+1}_{-0.7}$	1.6 ± 0.4	1.1 ± 0.2	0.8 ± 0.2	1.3 ± 0.2	1.57 ± 0.09
Ca[e]	5^{+6}_{-2}	5^{+2}_{-1}	3.3 ± 0.6	3 ± 2	2.7 ± 0.6	2.0 ± 0.3	1.7 ± 0.3	2.1 ± 0.3	2.5 ± 0.2
Fe[e]	12^{+27}_{-5}	9^{+3}_{-2}	4.0 ± 0.6	2^{+3}_{-1}	3.3 ± 0.7	1.0 ± 0.2	1.3 ± 0.2	1.5 ± 0.2	2.5 ± 0.2
Ni[e]	40^{+110}_{-20}	35^{+14}_{-9}	19 ± 4	20^{+27}_{-11}	17 ± 5	9 ± 3	7 ± 3	8 ± 2	14 ± 2
χ^2_ν	1.0	1.4	1.9	1.0	1.5	2.0	1.6	2.2	5.0
Mass[f]	0.3	1.4	5	1	12	15	18	12	...

Notes.—Results of spectral fitting, using the single temperature equilibrium model VMEKAL, and the absorption model WABS. All errors are 90% confidence. The regions used here are shown in Fig. 2. Units of right ascension are hours, minutes, and seconds, and units of declination are degrees, arcminutes, and arcseconds.

[a] This region encompasses the whole supernova remnant, and is thus shown for comparison. Note that the single temperature model is unacceptable for the whole SNR.

[b] The foreground column density is in units of 10^{22} cm^{-2}.

[c] The temperature is in units of keV (i.e., 1.2×10^7 K).

[d] $\int n_e n_H dV$ is in units of pc^3 cm^{-6}, and assumes a distance of 11.4 kpc.

[e] The number per hydrogen relative to solar values. Abundances of the elements not shown were all set to zero for this analysis.

[f] A very rough estimate of the mass, in solar masses, assuming a smooth medium. The depth of each region was assumed to be equal to its width.

trend can be seen in images of the dominant He-like and H-like emission lines (Si, S, Ar, Ca, Fe, and Ni), which are shown in Figure 3. We also extracted a 4–6 keV continuum image, which is morphologically similar to the Si, S, Ar, and Ca images.

We roughly estimated the total X-ray-emitting mass in each region, assuming uniform density and that the depth of each region was similar to its width. These mass estimates are also shown in Table 2. Note that these fits imply a total X-ray-emitting Fe mass on the rough order of $\frac{1}{10} M_\odot$. Also note that despite the clear abundance difference between west and east, the total Fe mass is approximately symmetrical between the east and the west.

3. DISCUSSION

The data presented here imply that W49 B is the result of an unusual explosion of a massive or supermassive star. The barrel-shaped structure, as seen in the 1.64 μm [Fe II] emission, is also seen in the high-pass-filtered radio maps of Moffett & Reynolds (1994), suggesting that the location of warm gas is correlated with high magnetic field. We interpret these as coaxial circular rings of enhanced density structures, such as is common in wind-blown bubbles (e.g., NGC 6888; Parker 1978). Most importantly, the [Fe II] emission defines the rotation axis of the progenitor star, which is inclined by 70° from the line of sight. Note that the [Fe II] emission arises from much cooler gas than the X-ray. We interpret the Fe^+ gas ([Fe II] emission) to be material from the progenitor's strong winds, while we interpret the H-like Fe (X-ray Fe lines) to most likely arise from ejecta (as discussed below in § 3.1).

The H_2 emission clearly shows a bow-shock structure in the southeast, emanating from the point of contact between the X-ray "jet" (§ 2.2) and the shell. The shock appears to have traveled a distance of 1.9 pc inside the molecular gas, the thickness of the southeastern H_2 emission. Assuming that the molecular cloud is uniform density, the shock speed must be less than 40 km s^{-1} in order to not dissociate the H_2. This velocity is consistent with an X-ray shock velocity of 1150 km s^{-1} multiplied by $(n_X/n_{H_2})^{1/2}$, where n_X is a density inferred from X-ray gas of 1–3.5 cm^{-3}, and n_{H_2} is an H_2 gas density of 3000 cm^{-3}; note that the velocity is inversely proportional to square root of the density ratio.

The complication with this interpretation is that it would take a 40 km s^{-1} shock 45,000 yr to travel the 1.9 pc that is the apparent thickness of the H_2 shell. Thus, either (1) the remnant actually is 45,000 yr old, (2) the thickness of the H_2 shell is much less than 1.9 pc, or (3) the shock is moving much faster than 40 km s^{-1}. Each of these possibilities has its own implications: (1) a 45,000 yr old remnant would have required a larger explosion energy and containment by the cavity to have such a high current X-ray temperature, (2) complex projection effects would need to be invoked to significantly reduce the distance the shock had to travel in the molecular gas, and (3) a magnetic precursor could propagate faster without dissociating the molecular hydrogen.

Elaborating on scenario (3), we can estimate the ionization fraction in the molecular cloud by assuming that the H_2 is excited by a magnetic precursor propagating at the ion-magnetosonic speed (v_{ims}), as in the Cygnus Loop (Graham et al. 1991) and some Herbig-Haro objects (e.g., McCoey et al. 2004). If we also assume equipartition between the magnetic and gas pressures, an age of about 2000 yr, and a sound speed of about 3 km s^{-1} (§ 2.1), the ionization fraction in the molecular cloud would be $2\rho_i/\rho \sim 10^{-5}$, because $v_{ims} \sim (B^2/4\pi\rho_i)^{1/2}$, where ρ_i is the ion mass density.

The *Chandra* (§ 2.2) and *XMM-Newton* (Miceli et al. 2006) data show Ni overabundances and concentrated Fe at the center, which also support the scenario of an explosion of a massive or supermassive star. We explore two viable interpretations for this morphology and chemical structure. The first interpretation (§ 3.1) is that W49 B resulted from a jet-driven explosion producing the jet, chemical structure, and H_2 bow-shock structure. The alternative interpretation (§ 3.2) is that the explosion was itself symmetrical, and the jet structure is rather the result of interactions between the shock and an enriched interstellar cloud.

3.1. *The Jet-driven Explosion Interpretation*

A mild consensus has formed regarding the nature of long/soft gamma-ray bursts (GRBs), i.e., that they are the result of a massive stellar collapse that produces a highly collimated relativistic blast wave along the poles of the rotation axis of the core of the progenitor star as it collapses to form a black hole

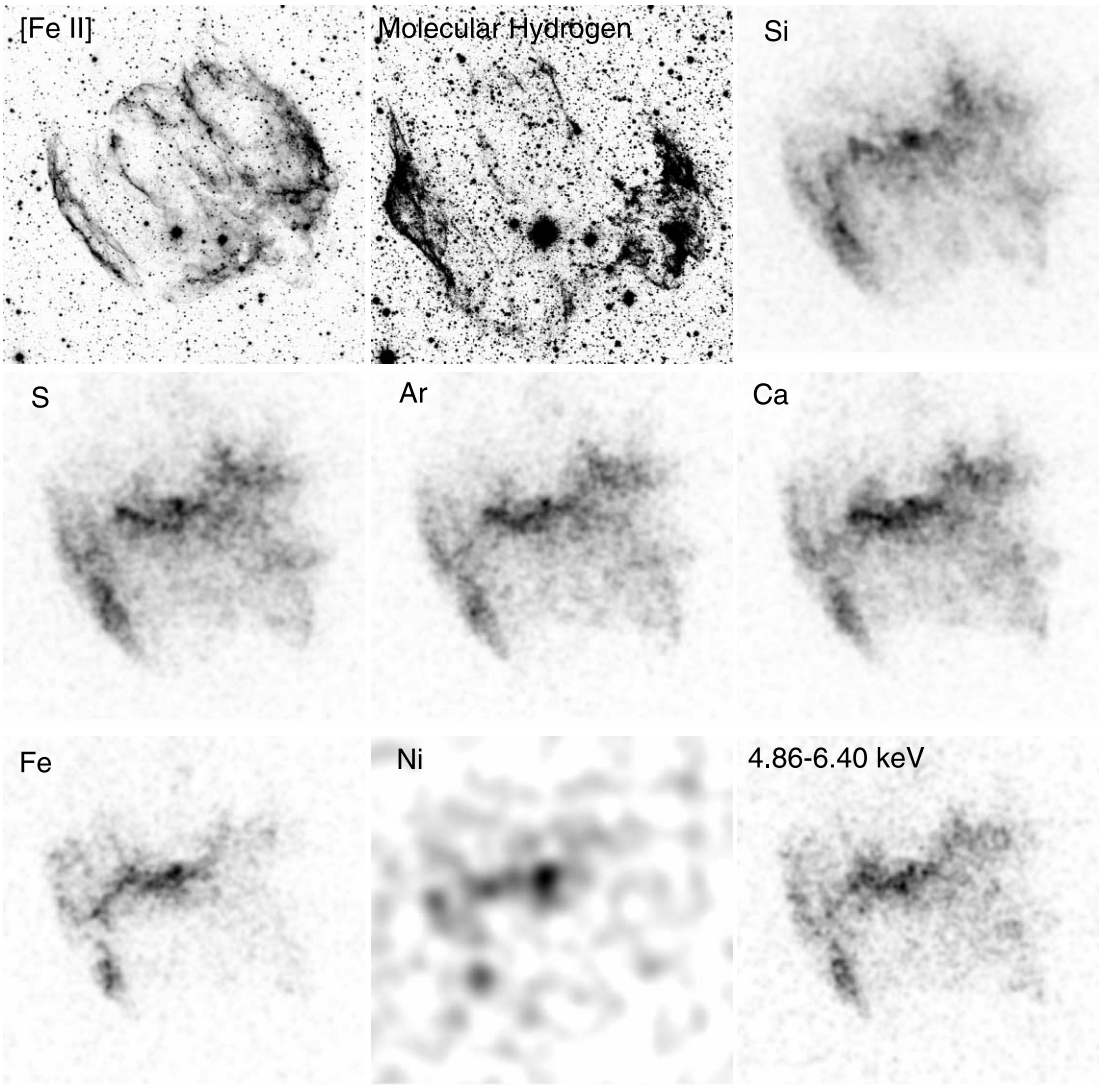

FIG. 3.—*Chandra* spectra emission line images for Si (1.65–2.1 keV), S (2.4–2.7 keV), Ar (3.0–3.35 keV), Ca (3.5–4.3 keV), Fe (6.0–7.2 keV), and Ni (7.35–8.1 keV). The images were Gaussian smoothed with $\sigma = 4$ pixels, except for Ni, which was smoothed with $\sigma = 16$ pixels because of its low count rate. For comparison, we also show the Palomar [Fe II] and H_2 images, as well as the *Chandra* 4.86–6.40 continuum image. The images are scaled linearly to the minimum and maximum surface brightness.

(Woosley & MacFadyen 1999; MacFadyen et al. 2001). This conical blast wave will continue moving forward until it becomes semirelativistic, at which point it will start expanding perpendicular to the jet (Rhoads 1997; Sari et al. 1999). This model has been applied successfully to the light curves of GRB afterglows, explaining the sharp steepening of the light curve when the shock slows down and $\Gamma < \theta_{\rm jet}$, where Γ is the Lorentz factor of the blast wave and $\theta_{\rm jet}$ is the opening half-angle of the jet, which are believed to be $\sim 10^\circ$ on average (Frail et al. 2001; Bloom et al. 2003). The distance that the jet travels, the "jet-break distance," depends on the mass it sweeps up, but this is typically a few parsecs. (At a distance of 11.4 kpc, the length of the jet region is about 4 pc, which would be W49 B's observed jet-break distance.)

The frequency of observed GRBs is approximately 1 per 10^7 yr per galaxy (Schmidt 1999). However, we only observe a fraction of the explosions f_b due to beaming effects, where $f_b = 1 - \cos(\theta_{\rm jet})$, increasing the rate to about 1 per 10^6 yr per galaxy, assuming the canonical 10° opening angle. Thus, depending on the length of time the distinguishing characteristics remain intact, it is possible that at least 1 remnant of a jet-driven explosion could be found in the Milky Way.

These explosions result from the most massive stars, so they should occur within the molecular clouds that formed them (Reichart & Price 2002). Given that the most massive stars go through phases of high mass-loss rate (e.g., luminous blue variable [LBV] phase) and fast stellar winds (e.g., Wolf-Rayet phase), one would also expect their remnants to be located inside bubbles within molecular clouds (Mirabal et al. 2003; Chevalier et al. 2004). Therefore, the distinguishing characteristics of a remnant of a jet-driven explosion inside a massive star should include the following: (1) a double T-shaped structure, which traces the path of the bipolar jets; (2) a higher abundance of heavy elements than a typical Type II SNR, because the jet originates from inside the iron core; (3) a supermassive progenitor with strong stellar winds; and (4) the nonexistence of a neutron star. Evidence for these include (1) the double T-shaped structure is observed in the X-ray images (see Figs. 1 and 3, and the figures in Miceli et al. 2006) and the radio maps (Moffett & Reynolds 1994); (2) *Chandra* (§ 2.2) and *XMM-Newton* (Miceli et al. 2006) both observe an

overabundance of Ni and Fe in the center and jet regions; (3) the infrared images show evidence for past stellar winds interacting with a dense circumstellar medium, as would be expected from a supermassive progenitor; and (4) there is no evidence for a neutron star in the *Chandra* data.

When the star collapses, the resulting twin jets emerge from the poles, leaving behind material from the stellar core, and thus explaining the enhanced abundances in the center, jet, and eastern shell regions (§ 2.2; Miceli et al. 2006). The jet continues until it encounters enough mass to slow to semirelativistic speeds (i.e., it "breaks"), which will happen at the bubble wall, if not before, because of the large density of the molecular cloud. This will result in both a shock transmitted into the dense bubble and a shock reflected back into the cavity. The morphology of W49 B (Fig. 1) suggests that the southeastern jet broke at the bubble wall, while the northwestern jet broke before hitting the bubble wall. This interpretation would explain the clear morphological structure of the southeastern jet, as well as the more complex northwestern jet. This hypothesis also explains the relative brightness of the western [Fe II] emission compared to the X-ray, implying cooler gas in the west as observed here and by Miceli et al. (2006). This is also consistent with the observed ^{13}CO map of Simon et al. (2001), which shows more molecular gas to the north and west of W49 B than the south and east. Moreover, an early western jet-break would also dilute the ejecta, explaining the lower abundances in the west compared to the east, yet there should be about the same Fe mass overall, which is observed (Table 2).

An issue to consider is the short cooling time of [Fe II], which requires a continuous heating source for the Fe^+ gas. Thus, either the Fe^+ shell is currently being shocked, or it is gaining energy from the adjacent X-ray-emitting hot plasma. The thermal energy currently contained in the X-ray plasma is much greater than the thermal energy in Fe^+ (only about 10^{45} ergs), so this seems plausible.

3.2. *The Supernova Interpretation*

An isotropic explosion inside a wind-blown bubble could also produce these observations, assuming a unique structure of the surrounding medium. The obvious problem, however, is the clear bipolar structure in the infrared data images. A solution may be a strong and ordered magnetic field, which is consistent with W49 B's high radio surface brightness, the radio and [Fe II] hoop morphology, and the possible magnetic precursor in the H_2 cloud.

The X-ray jet morphology and abundance variations could possibly be explained under this model by postulating a metallically-enriched clump of fast-moving ejecta that was overtaken by one of the supernova shocks. The shock would break up the clump, spreading the material in a line parallel to the shock velocity. Thus, the resulting density enhancement would be elongated radially and would have an overabundance of heavy elements.

Miceli et al. (2006) compare W49 B to the SNR G292.08+1.8, which has an apparently similar X-ray morphology, but has been interpreted to contain a disk or torus of material viewed edge-on (Park et al. 2004). We disfavor this interpretation for W49 B, because the axis of the torus would need to be perpendicular to the axis of the bipolar wind structures presented here, so they could not have been caused by the same progenitor star.

Another advantage of the supernova model is that W49 B's abundances are more consistent with the 25 $M_\odot$ models of Maeda & Nomoto (2003) than their 40 $M_\odot$ hypernova models (Miceli et al. 2006). However, given the infancy of detailed GRB models in 2003, and the more important chemical morphology, we believe this argument to be weak.

This interpretation has the advantage that traditional supernova explosions, inside complex cloud regions, are common, well-known occurrences. On the other hand, its primary flaw is that it posits particular cloud configurations to explain particular morphological structures.

4. CONCLUSION

We have presented evidence that W49 B resulted from the explosion of a supermassive star, inside a wind-blown bubble, which is in turn interior to a dense molecular cloud. We have also given two interpretations for its morphological and chemical structure, each explanation requiring a set of extreme initial conditions. One interpretation assumes that the axially symmetric structure is caused by the explosion mechanism, resulting in the conclusion that W49 B was a jet-driven explosion akin to the current model of long/soft gamma-ray bursts. The other interpretation assumes that the same observations were rather dominated by complex cloud and magnetic field structures, and that the explosion could have been a standard isotropic supernova explosion.

Future work should consist of detailed modeling, with a realistic preexplosion medium and with jet-driven and isotropic explosions, to explain all aspects of the W49 B observations.

Additional observations would also be useful, especially in order to understand complete yields of nucleosynthesis with infrared spectroscopy by complementing the yields of the X-ray gas and to independently map out the molecular cloud structure surrounding W49 B.

We are grateful to L. Rudnick, who participated in the observing run and contributed significant insight. We are grateful to J. Hester, T. Pannuti, and W. Tucker for insightful discussions. We also thank R. Petre for discussions on W49 B prior to this work. Support for this work was provided by NASA through LTSA grant NRA-01-01-LTSA-013 and *Chandra* award GO3-4070C awarded to J. Rho.

REFERENCES

Bloom, J. S., Frail, D. A., & Kulkarni, S. R. 2003, ApJ, 594, 674
Brogan, C. L., & Troland, T. H. 2001, ApJ, 550, 799
Chevalier, R. A. 1999, ApJ, 511, 798
Chevalier, R. A., Li, Z., & Fransson, C. 2004, ApJ, 606, 369
Cox, D. P., Shelton, R. L., Maciejewski, W., Smith, R. K., Plewa, T., Pawl, A., & Różyczka, M. 1999, ApJ, 524, 179
Frail, D. A., et al. 2001, ApJ, 562, L55
Graham, J. R., Wright, G. S., Hester, J. J., & Longmore, A. J. 1991, AJ, 101, 175
Gwinn, C. R., Moran, J. M., & Reid, M. J. 1992, ApJ, 393, 149
Hamilton, A. J. S., Chevalier, R. A., & Sarazin, C. L. 1983, ApJS, 51, 115
Hwang, U., Petre, R., & Hughes, J. P. 2000, ApJ, 532, 970
Lacey, C. K., Lazio, T. J. W., Kassim, N. E., Duric, N., Briggs, D. S., & Dyer, K. K. 2001, ApJ, 559, 954
Liedahl, D. A., Osterheld, A. L., & Goldstein, W. H. 1995, ApJ, 438, L115
MacFadyen, A. I., Woosley, S. E., & Heger, A. 2001, ApJ, 550, 410
Maeda, K., & Nomoto, K. 2003, ApJ, 598, 1163
McCoey, C., Giannini, T., Flower, D. R., & Caratti o Garatti, A. 2004, MNRAS, 353, 813
Mewe, R., Gronenschild, E. H. B. M., & van den Oord, G. H. J. 1985, A&AS, 62, 197
Mewe, R., Lemen, J. R., & van den Oord, G. H. J. 1986, A&AS, 65, 511
Miceli, M., Decourchelle, A., Ballet, J., Bocchino, F., Hughes, J. P., Hwang, U., & Petre, R. 2006, A&A, 453, 567
Mirabal, N., et al. 2003, ApJ, 595, 935
Moffett, D. A., & Reynolds, S. P. 1994, ApJ, 437, 705
Morrison, R., & McCammon, D. 1983, ApJ, 270, 119

Park, S., Hughes, J. P., Slane, P. O., Burrows, D. N., Roming, P. W. A., Nousek, J. A., & Garmire, G. P. 2004, ApJ, 602, L33
Parker, R. A. R. 1978, ApJ, 224, 873
Petre, R., Hwang, U., & Holt, S. S. 2000, BAAS, 32, 1236
Pye, J. P., Thomas, N., Becker, R. H., & Seward, F. D. 1984, MNRAS, 207, 649
Reichart, D. E., & Price, P. A. 2002, ApJ, 565, 174
Rho, J., Jarrett, T. H., Cutri, R. M., & Reach, W. T. 2001, ApJ, 547, 885
Rho, J., & Petre, R. 1998, ApJ, 503, L167
Rhoads, J. E. 1997, ApJ, 487, L1
Sari, R., Piran, T., & Halpern, J. P. 1999, ApJ, 519, L17
Schmidt, M. 1999, ApJ, 523, L117
Seward, F., Smith, R., Hagler, J., Portolese, L., Gaetz, T., Slane, P., Koo, B.-C., & Lee, J.-J. 2004, in IAU Symp. 218, Young Neutron Stars and Their Environments, ed. F. Camilo & B. M. Gaensler (San Francisco: ASP), 93
Shelton, R. L., Cox, D. P., Maciejewski, W., Smith, R. K., Plewa, T., Pawl, A., & Różyczka, M. 1999, ApJ, 524, 192
Simon, R., Jackson, J. M., Clemens, D. P., Bania, T. M., & Heyer, M. H. 2001, ApJ, 551, 747
Stahle, C. K., Petre, R., Hwang, U., Harrus, I. M., & Holt, S. S. 2001, in ASP Conf. Ser. 251, New Century of X-ray Astronomy, ed. H. Inoue & H. Kunieda (San Francisco: ASP), 278
White, R. L., & Long, K. S. 1991, ApJ, 373, 543
Wilson, J. C., et al. 2003, Proc. SPIE, 4841, 451
Woosley, S. E., & MacFadyen, A. I. 1999, A&AS, 138, 499